Ballistic transport through coupled T-shaped quantum wires

Yuh-Kae Lin, Kao-Chin Lin, Der-San Chuu*

Department of Electrophysics, National Chiao Tung University, 1001 Ta Hsueh Road, Hsinchu 30050, Taiwan

Abstract

The ballistic conductance of a coupled T-shaped semiconductor quantum wire (CTQW) is studied. Two types of CTQW are considered, one of which is a Π-shaped quantum wire (ΠQW) which consists of two vertical arms on the same side of the horizontal arm and the other a Π-clone quantum wire (ΠCQW) which consists of two vertical armes on the opposite sides of the horizontal arm. The mode matching method and Landauer-Buttiker theory are employed to study the energy dependence of the ballistic conductance. Most of transmission profiles of ΠQW and ΠCQW are found to be distinguishable for large separation d between the two vertical arms. The transmission probability manifests oscillatory behavior when d is increased. When a potential is applied to the connection region, it results in decoupling or coupling effects between the two T-shaped quantum wires according to whether it is positive or negative. When magnetic field is applied to CTQW, the transmission profiles are found to be affected prominently even if the electron passes through the field free region only.

1. Introduction

Recently, the development in microetching and epitaxial growth techniques has made the fabrication of semiconductor nanostructures successful. Such nanostructures include T-shaped quantum wires in which quasi-one-dimensional confinement is achieved at the intersection of two quantum wells. Both experimental and theoretical studies on the nonlocal ballistic transport of these structures have been stimulated. In general, T-shaped quantum wires can be fabricated by using the cleaved-edge-overgrowth (CEO) technique. The vertical arms are first grown as alternating GaAs/Al$_x$Ga$_{1-x}$As multilayers on a (0 0 1) substrate by molecular beam epitaxy. The resulting crystal is then cleaved along a plane orthogonal to the vertical arms, and a new layer of GaAs quantum well is finally grown over the exposed (1 1 0) surface to form the horizontal arm. The array of T-shaped regions can confine the carrier wavefunctions in several tens of angstroms. This technique can be also employed to fabricate other electron stub tuners (ESTs), e.g. Π-shaped (i.e. 2 vertical arms and one horizontal arm) quantum well. T-shaped quantum wires (TQW) possess some improved optical properties of one dimensional excitons, such as the excitonic laser emission [1,2], the enhancement of excitonic binding energy [3–6], and the concentrated oscillator strength [4–7]. The

*Corresponding author. Tel.: +886-3-5712-121; fax: +886-3-5725230.

E-mail address: dschuu@cc.nctu.edu.tw (D.-S. Chuu).

conductance of such a mesoscopic structure exhibits many peculiar and interesting features due to its intrinsic nonlocality. Quantum conductance in mesoscopic structures is the consequence of a complex scattering process which involves the boundary and the shape of the potential across the structural geometry as a whole.

Several studies on the electronic transmission properties of a T-shaped quantum structure have been carried out [7–14]. Many interesting transmission characteristics, such as resonant transmission and resonant reflection in the T-shaped structures have been predicted. Such behaviors are known to be caused from the quantum interference which dominates the ballistic transport regime. Theoretically, one may view the resonance as being mediated by the quasibound states of the system. The system of T-shaped quantum wires possesses open geometry, therefore, the injected carriers that travel ballistically over the wire region will cross the wire region and show a strong energy dependent transmission as a consequence of quantum interference effect induced by the interplay between the propagating modes of the wires.

By using the scattering matrix approach and Landauer-Buttiker theory, Goldoni et al. [11] have calculated the conductance of T-shape and coupled T-shaped quantum wires with different wire widths. The transmission coefficient of the whole coupled T-shaped quantum wires can be obtained easily since the total T-matrix is the product of the T-matrices of isolated wires. The double resonance obtained in their result is ascribed to a fingerprint of the bonding and antibonding combinations of the resonance states of isolated wires. Bohn [12] has introduced a periodic array of T-shaped devices and showed that deflected arrays exhibited a unique resonance structure with respect to electrons travelling along the array. The coefficients of the reflection and transmission through the array can peak simultaneously at resonance. Unlike the analogous case in superlattices, the peaks are at energies where the wavelength λ satisfies the condition $n\lambda/2 = d$ for some integer n. Consequently, the scattering wave function possesses nodes at the intersection of the horizontal arm and the vertical arm, and thus

greatly reduces the flux lost to vertical leads. Nikolic and Sordan [13] have also studied the transmission properties of a quantum waveguide system with attached stubs in the ballistic regime. They found the transconductance and the differential drain conductance were small. Their result suggested limited abilities for conventional application of the transistor. Chen et al. [14] calculated transmission of electrons in a T-shaped open quantum waveguide (TOQW) in presence of an inhomogeneous magnetic field perpendicular to the TOQW plane with mode-matching technique. The transmission profiles were found to depend sensitively on geometric parameters.

In this work, we study a Π-shaped open quantum structure and its clone shape (i.e. one of the vertical arms is on the other side of the horizontal arm), which are four-terminal waveguide-like structures, schematically as shown in Fig. 1. These structures can be fabricated by the CEO technique. The Π-shaped and its clone opened quantum structures can be also fabricated on a heterostructure comprising a single $Al_xGa_{1-x}As/GaAs$ interface grown on undoped GaAs by molecular beam epitaxy. The AlGaAs layer is silicon doped and a thick spacer layer separated the 2D electron gas from the doped AlGaAs layer. The ESTs are defined by four Schottky gates patterned by electron beam lithography to form a Π-shape or its clone shape on the surface of the wafer. In our calculation, we take first the geometric variation into account. Second, the interconnection region is considered to be acted by a potential. Third, the magnetic field is considered to apply to the vertical wires. Unlike the stubs, arms of the structures considered in our
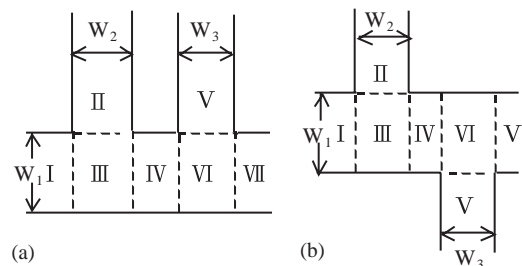

Fig. 1. (a) The schematic illustrations of the geometries of a ΠQW system. (b) A ΠCQW system.

case are assumed to be long enough and open in the horizontal and the vertical directions. The centers of the two vertical arms are spaced by a distance d as shown in Fig. 1. The scattering matrices are calculated by using mode-matching method. Our model will be presented briefly in the next section. Results and discussions will be given in the final section.

2. Model and formalism

The structure is modeled as illustrated in Fig. 1: It contains a horizontal wire including regions I, III, IV, VI, VII and has a width W_1, two vertical wires with width W_2 (W_3) for region II (V), an interconnection part for region IV and a junction region with an area of $W_1 \times W_2$ ($W_1 \times W_3$) for region III (VI). Inside the wires, 2DEG system with perfect barrier confinement (e.g. high quality interfaces) is assumed. The individual electron propagates ballistically through the entire wire. The transverse potential inside the wire is set to zero.

The whole quantum wire can be split into several individual homogeneous subregions as shown in Fig. 1. The two intersection regions III and VI act as scattering centers. And the interconnecting region IV acts as a connection of the two TQWs. An nth mode electron is considered to inject from left of region I into the wire. The wave function in region I can be written in terms of a sum of incident and reflecting modes as

$$\Psi_n^{\mathrm{I}}(x,y) = \Phi_n^{\mathrm{I}(+)}(y)\mathrm{e}^{ik_n^{\mathrm{I}(+)}(x+0.5W_2)} + \sum_m R_{mn}\Phi_m^{\mathrm{I}(-)}(y)\mathrm{e}^{ik_m^{\mathrm{I}(-)}(x+0.5W_2)}, \quad (1)$$

where $k_n^{\mathrm{I}(\pm)} = \sqrt{k^2 - (n\pi/W_1)^2}$, $\pm$ represents the incident or reflecting mode, respectively, and $\Phi_n^{\mathrm{I}(\pm)}$ are envelope functions in region I. The wave functions in regions II, V, and VII are given by a sum of outgoing modes respectively, i.e.,

$$\Psi_n^{\mathrm{II}}(x,y) = \sum_m S_{mn}^{(1)}\Phi_n^{\mathrm{II}(+)}(x)\mathrm{e}^{ik_m^{\mathrm{II}(+)}(y-0.5W_1)}, \quad (2)$$

$$\Psi_n^{\mathrm{V}}(x,y) = \sum_m S_{mn}^{(2)}\Phi_m^{\mathrm{V}(\pm)}(x)\mathrm{e}^{ik_m^{\mathrm{V}(\pm)}(y\mp0.5W_1)}, \quad (3)$$

where $\pm$ represents the upward or downward arm and by use of $x' = x + d$

$$\Psi_n^{\mathrm{VII}}(x',y) = \sum_m T_{mn}\Phi_m^{\mathrm{VII}(+)}(y)\mathrm{e}^{ik_m^{\mathrm{VII}(+)}(x'-0.5W_3)}. \quad (4)$$

The wave function in region IV is given by the sum of rightgoing (+) and leftgoing (−) modes,

$$\Psi_n^{\mathrm{IV}}(x,y) = \sum_m [U_{mn}\Phi_m^{\mathrm{IV}(+)}(y)\mathrm{e}^{ik_m^{\mathrm{IV}(+)}(x-0.5W_2)} + V_{mn}\Phi_m^{\mathrm{IV}(-)}(y)\mathrm{e}^{ik_m^{\mathrm{IV}(-)}(x-0.5W_2)}]. \quad (5)$$

In region III and region VI, all modes must be taken into account, thus

$$\Psi_n^{\mathrm{III}}(x,y) = \sum_j f_j(y)[a_{jn}\sin(k_j'(x-0.5W_2)) + b_{jn}\sin(k_j'(x+0.5W_2))] + \sum_j g_j(x)c_{jn}\sin(k_j''(y+0.5W_1)), \quad (6)$$

$$\Psi_n^{\mathrm{VI}}(x',y) = \sum_j f_j(y)[d_{jn}\sin(k_j'(x'-0.5W_3)) + e_{jn}\sin(k_j'(x'+0.5W_3))] + \sum_j g_j'(x')h_{jn}\sin(k_j'''(y\pm0.5W_1)).$$

$$(7)$$

Here $f_j(y) = \sqrt{(2/W_1)}\sin((j\pi/W_1)(y+0.5W_1))$, $g_j(x) = \sqrt{(2/W_2)}\sin((j\pi/W_2)(x+0.5W_2))$ and $g_j'(x') = \sqrt{(2/W_3)}\sin((j\pi/W_3)(x'+0.5W_3))$ represent the transverse wave functions of the electron in mode j inside different regions of the wires, and are used as the expansion basis. The wave numbers $k_j' = \sqrt{k^2 - (j\pi/W_1)^2}$, $k_j'' = \sqrt{k^2 - (j\pi/W_2)^2}$, and $k_j''' = \sqrt{k^2 - (j\pi/W_3)^2}$ are either real for propagating modes or pure imaginary for evanescent modes.

Now expand the wavefunctions in terms of a set of complete bases corresponding to the transverse eigenfunctions in regions I, II, IV, V and VII, respectively as $\Phi_n^{\mathrm{I}(\pm)}(y) = \sum_j \alpha_{jn}^{\mathrm{I}(\pm)}f_j(y)$, $\Phi_m^{\mathrm{II}(+)}(x) = \sum_j \beta_{jn}^{\mathrm{II}(+)}g_j(x)$, $\Phi_m^{\mathrm{IV}(\pm)}(y) = \sum_j \gamma_{jm}^{\mathrm{IV}(\pm)}f_j(y)$, $\Phi_n^{\mathrm{V}(\pm)}(x') = \sum_j \delta_{jn}^{\mathrm{V}(\pm)}g_j'(x')$, and $\Phi_n^{\mathrm{VII}(+)}(y) = \sum_j \zeta_{jn}^{\mathrm{VII}(+)} f_j(y)$. And substituting these functions into Eq. (1) for a given Fermi energy E_{F}, we obtain five sets of

eigen-wave-numbers $\{k_n^{\mathrm{I}(\pm)}\}$, $\{k_n^{\mathrm{II}(+)}\}$, $\{k_n^{\mathrm{IV}(\pm)}\}$ $\{k_n^{\mathrm{V}(\pm)}\}$, and $\{k_n^{\mathrm{VII}(+)}\}$ and eigen-wave-functions $\{\Phi_n^{\mathrm{I}(\pm)}(y)\}$, $\{\Phi_n^{\mathrm{II}(+)}(y)\}$, $\{\Phi_n^{\mathrm{IV}(\pm)}(y)\}$, $\{\Phi_n^{\mathrm{V}(\pm)}(y)\}$, and $\{\Phi_n^{\mathrm{VII}(+)}(x)\}$. By using boundary matching technique, [15] we can derive all coefficients in Eqs. (2)–(7) such as $\{r_{mn}\}$, $\{s_{mn}^{(1)}\}$, $\{s_{mn}^{(2)}\}$, $\{u_{mn}\}$, $\{v_{mn}\}$, $\{t_{mn}\}$, $\{a_{jn}\}$, $\{b_{jn}\}$, $\{c_{jn}\}$, $\{d_{jn}\}$, $\{e_{jn}\}$, and $\{h_{jn}\}$.

The transmission probabilities $\tilde{t}_{nj}$ (in region VII) and $\tilde{s}_{nj}^{(1)}(\tilde{s}_{nj}^{(2)})$ (in region II and region V) from the incident mode n to the final mode j, and the reflection probability $\tilde{r}_{nj}$ from the incident mode n to the final mode j (in region I) can be obtained, respectively, as follows: $\tilde{r}_{nj} = V_j^{\mathrm{I}(-)}/V_n^{\mathrm{I}(+)}|r_{nj}|^2$, $\tilde{s}_{nj}^{(1)} = V_j^{\mathrm{III}(+)}/V_n^{\mathrm{I}(+)}|s_{nj}^{(1)}|^2$, $\tilde{s}_{nj}^{(2)} = V_j^{\mathrm{III}(+)}/V_n^{\mathrm{I}(+)}|s_{nj}^{(2)}|^2$, and $\tilde{t}_{nj} = V_j^{\mathrm{II}(+)}/V_n^{\mathrm{I}(+)}|t_{nj}|^2$.

It should be emphasized that the expansion of the wavefunction in terms of a set of complete basis corresponding to the transverse eigenfunctions involves an infinite sum including all possible evanescent modes. In practice, in order to solve this set of equations numerically, we have to truncate the sum at some finite number which should be large enough to achieve a desired accuracy. The numerical convergence can be checked by flux conservation, i.e. the relationship $\sum_j (\tilde{t}_{jn} + \tilde{r}_{jn} + \tilde{s}_{jn}) = 1$ should be fulfilled accurately.

The total transmission coefficients T and S are then given by

$$T = \sum_{n=1}^{N_1} \sum_{j=1}^{N_2} \tilde{t}_{nj}, \tag{8}$$

$$S = \sum_{n=1}^{N_1} \sum_{j=1}^{N_3} \tilde{s}_{nj}, \tag{9}$$

where N_1, N_2 and N_3 are the numbers of propagating modes in regions I, II and III, respectively. The conductance G at zero temperature is given by the Landauer–Buttiker formula:

$$G_t = (2e^2/h)T \tag{10}$$

and

$$G_s = (2e^2/h)S. \tag{11}$$

3. Numerical results and discussions

3.1. Transmission properties with geometric variations

We present our results in terms of some convenient parameters: (1) the first threshold energy $E_1 = (\hbar^2/2m^*)(\pi/W_1)^2$ through horizontal wire, (2) the distance d between two centers of the intersections of vertical wires and horizontal wire, (3) the ratios of widths $\alpha = W_2/W_1$ and $\gamma = W_3/W_1$.

First of all, we consider that all wires have the same width, namely W. Transmission probabilities are calculated with varying k_{F} as shown in Figs. 2(a) and (b) for different d. Curves from bottom to top in Figs. 2(a) and (b) are shifted by 1.0 for clarity. Hereafter, we present the transmission probabilities of the ΠQW system as solid lines and those of the ΠCQW system as the dotted lines in all figures.

For $d = 1$, the vertical wires are adjacent to each other. Thus, a ΠQW with $d = 1$, can be regarded as a TQW with a double width in the vertical arm except there is an infinite thin wall along the vertical arm axis. However, one can note from the figure that the profiles of transmission of a ΠQW with $d = 1$ are quite different from the transmission profiles of a TQW with the same width $(2.0W_1)$ of the vertical arm [7]. In fact, the bottom curve of ΠQW $(d = 1)$ is similar to the result obtained in TQW with a vertical arm of $1.0W_1$ in width as Ref. [7]. This implies that the two systems are similar except the transmission amplitude is suppressed in a ΠQW system. For the ΠCQW, the sharp dip at $k_{\mathrm{F}} = 2.0\pi/W_1$ is replaced by a wider valley at a k_{F} precedes the value of $2.0\pi/W_1$. The transmission behaviors of the two structures (ΠQW and ΠCQW) are different in general, however, their periodic oscillations are the same. The period of the oscillation is dominated by the distance d as can be seen from Fig. 2. The periodicity can be fitted as $n\lambda_l = 2d$ approximately, where n is the number of periods in one mode, and $\lambda_l = 2\pi/(k_{\mathrm{F}} - \pi/W_1)$ denotes the longitudinal wave length of the incident electron waves. Thus, once one finds two peaks in the region $1.0 < k_{\mathrm{F}}W_1/\pi < 2.0$ for $d = 1W_1$, then four
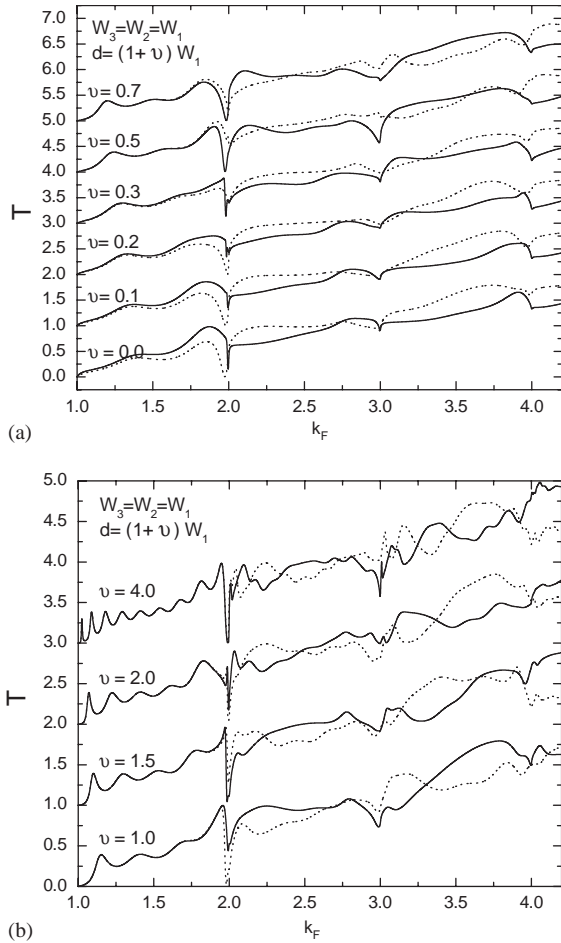
Fig. 2. The transmission T versus k_F for different d which is converted to v by $d = (1 + v)W_1$. All wires have same width. (a) $d < 2W_1$ (b) $d \geqslant 2W_1$. The solid lines represent the T of ΠQW, while the dotted lines represent the T of ΠCQW. Two consecutive curves have been offset vertically for clarity.

peaks will be found for $d = 2W_1$, and so on. Curves in both structures (ΠQW and ΠCQW) possess peak-dip structures. Especially, these peak-dip structures are more clear for larger d at $k_F = 2.0\pi/W_1$. On the contrary, they are observed only in certain circumstance for smaller d. According to the previous result [7], there exists a localized state in the intersection region for a symmetric TOQW with same wavenumber $k_F = 2.0\pi/W_1$. The peak-dip structure at $k_F = 2.0\pi/W_1$ can be ascribed to this localized state. The peak-dip structure is found at $k_F = 2.0\pi/W_1$ on the curve with $d = 1.5$

for ΠCQW. For d larger than $1.5W_1$, the peak-dip structure is sharper in ΠCQW than that in ΠQW.

Due to the fact that both ΠQW and ΠCQW structures are equivalent to a system of two TQWs, one may expect that the transmission properties of these two structures will be the same if the coupling between the constituent TQWs becomes very weak. However, our result does not manifest this accordance. On the contrary, the two transmission profiles are still distinguishable from each other even for large d. It is also found that the transmission probabilities vary periodically with d for a fixed wavenumber as shown in Fig. 3. These behaviors are the essential characteristics of ballistic theory.

Now let us consider the case that the widths of the vertical wires are the same, while the ratio of the width of vertical wire to horizontal wire is varied. The result is displayed in Fig. 4. For
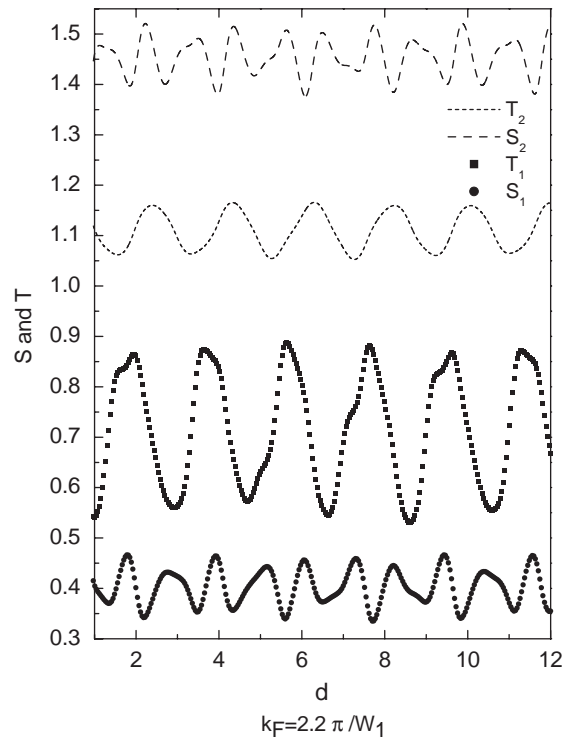

Fig. 3. The periodic behaviors of transmissions versus d for $W_3 = W_2 = W_1$. $T_1(T_2)$, $S_1(S_2)$ represent the total transmission coefficients T and S as defined in Eqs. (8) and (9) for ΠQW (ΠCQW). The result is obtained at the wavevector $k_F = 2.2\pi/W_1$.
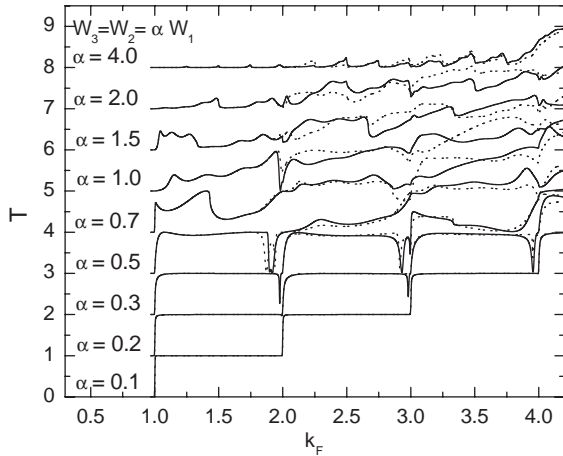
Fig. 4. Transmission versus k_F for different α. Where α is the ratio of the width of the vertical arm to the horizontal arm. And $d = 2\alpha W_1$. The solid lines represent the T of ΠQW, while the dotted lines represent the T of ΠCQW. Two consecutive curves have been offset vertically for clarity.

simplicity, we define the ratio of the width of vertical wire to horizontal wire as $\alpha = W_2/W_1 = W_3/W_1$. And the distance d is set to $2\alpha W_1$. For extremely small α, perfect stepwise profiles are observed in both structures. The transmissions are strongly suppressed when the ratio α is large (e.g. 2.0 and 4.0). The solid curve for $\alpha = 0.5$ agrees with the result of previous work [11]. A double resonance is evident either on the curve of $\alpha = 0.3$ or the curve of $\alpha = 0.5$. They are the signature of the bonding and antibonding combinations of the resonant quasi-1D state of isolated wires.

Finally, the transmission profiles in the ΠQW and ΠCQW with vertical wires of different width are considered. For simplicity, the width of one vertical wire is kept to be the same as that of the horizontal wire. The calculated transmission profiles for $W_1 = W_3$ and different W_2 are shown in Fig. 5(a) and those for $W_1 = W_2$ and various W_3 are shown in Fig. 5(b). Curves from bottom to top correspond to the cases of various $\alpha = W_2/W_1(W_3/W_1)$. It is observed that the transmission probability is drastically suppressed for large α as can be seen from the upper curves of Figs. 5(a) and (b). Comparing curves of Figs. 5(a) and (b), we observe that the transmission profiles are the same. When α is small, the transmission profiles of
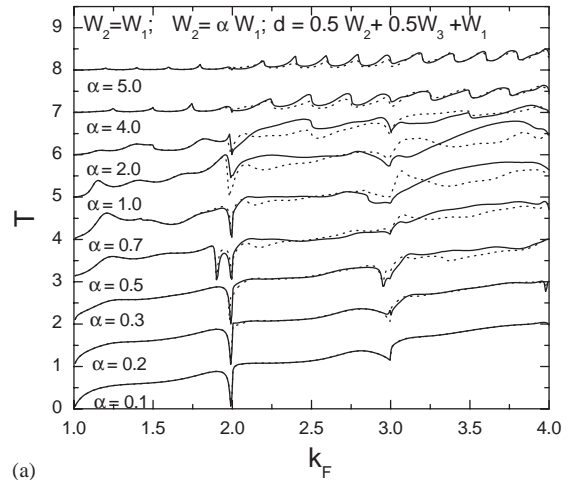
(a)
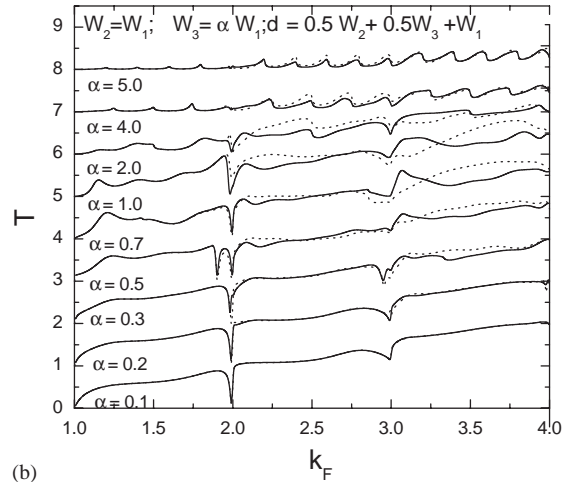
(b)

Fig. 5. Same as Fig. 2, except the width of one vertical arm varies. (a) The width of W_2 varies, (b) the width of W_3 varies. The solid lines represent the T of ΠQW, while the dotted lines represent the T of ΠCQW. Two consecutive curves have been offset vertically for clarity.

the ΠQW and ΠCQW become indistinguishable and almost the same as that of TQW system. The double resonance can be observed again.

3.2. Transmission under an additional potential

We now consider the case that an additional scalar potential is applied to the interconnection region IV. The applied potential can be negative or positive in according to its attraction or depletion

on the electrons. The different coupling profiles are interesting and may be important for practical usage of the mesoscopic devices.

Fig. 6 presents the calculated transmission profiles for different potential strength V_4 in unit of E_1. Here we consider $W_3 = W_2 = W_1$, and $d = 2W_1$. Figs. 6(a) and (c) correspond to the positive potential for electrons. Figs. 6(b) and (d) correspond to negative potential. As shown in Fig. 6(a), one can observe that the positive potential does not affect the transmission very much when $V_4 \leqslant E_1$. From Figs. 6(a) and (c), two features are shown: (1) the onset is shifted due to the depletion potential; (2) the positions of transmission dips are not changed. On the contrary, Figs. 6(b) and (d) show that the additional negative potential affects the transmission much stronger than the positive one. Especially, the potential enhances the coupling between the two TOQWs as one can note from the fact that the resonant dip-peak-dip structure becomes broader and shallower when the potential is increased. More peaks are on the curves and the positions of dips are not changed as the case of positive potential. Moreover, it can be observed that discrepancy between the two structures becomes prominent as the potential strength is increased. These results manifest that the negative potential increases the coupling strength between the two individual TOQWs.

3.3. Transmissions under the influence of surrounding magnetic fields

Finally, magnetic fields are considered to apply to the vertical wires only, therefore, the electrons
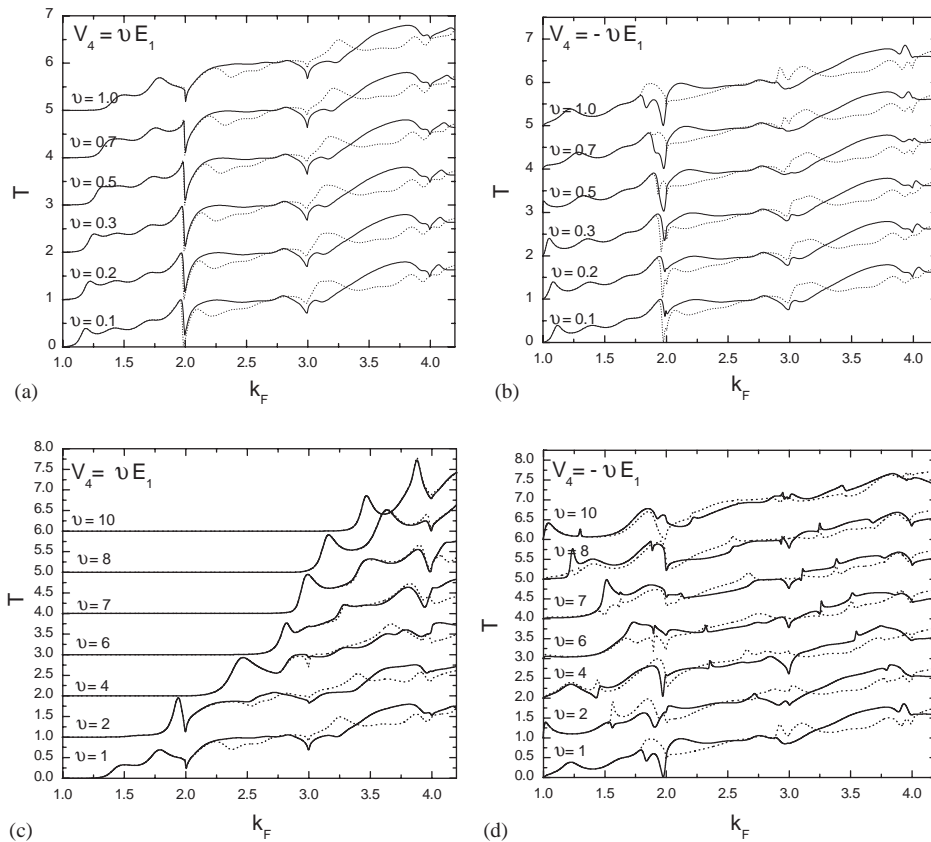

Fig. 6. Transmission profiles versus k_F for a potential V_4 applied to the region IV. (a) and (c) correspond to the positive potential and (b) and (d) correspond to the negative potential. The solid lines represent the T of ΠQW, while the dotted lines represent the T of ΠCQW. Two consecutive curves have been offset vertically for clarity.

pass through the main arm regions with no additional field. We shall study the effect of the surrounding magnetic fields on the transmission behavior. First, we consider the magnetic field is applied only to one of the vertical wires, i.e on arm II or arm V. The direction of the field is perpendicular to the 2DEG plane. Transmission probabilities are calculated as a function of Fermi wave vector as depicted in Fig. 7. Curves in Fig. 7(a) are offset for clarity, and correspond to the cases of different magnetic field strength. Those shown in Fig. 7(b) are the same except the magnetic field is applied to region V. From these
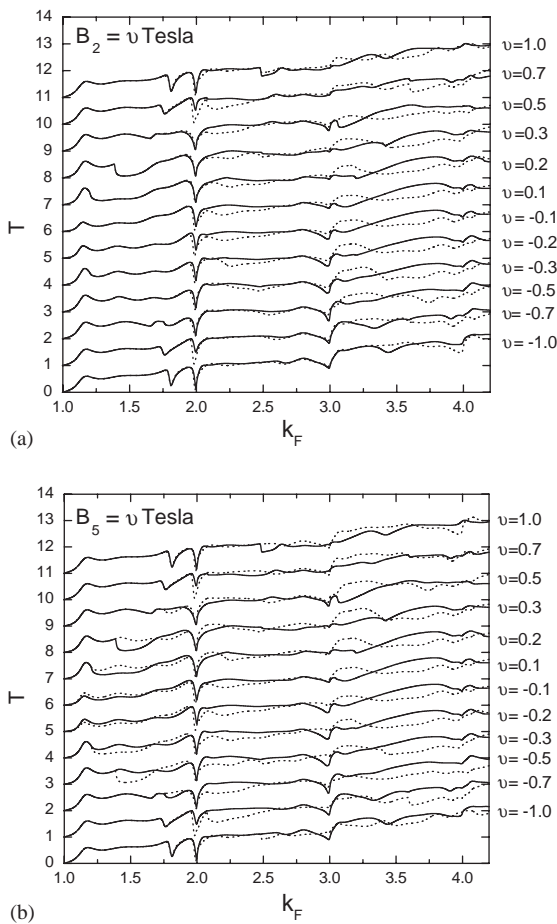

Fig. 7. Transmission profiles versus k_F for the magnetic field applied to only one vertical arm. (a) to region II, and (b) to region V. The solid lines represent the T of ΠQW, while the dotted lines represent the T of ΠCQW. Two consecutive curves have been offset vertically for clarity.

curves, one can conclude that: (1) the magnetic field does affect the transmission, although the electrons do not pass through the region with magnetic field directly. This phenomenon accords with Aharonov-Bohm effect. However, no periodic behavior can be found. This is because that all incident electrons passing by the magnetic field in the same side, therefore, no self-interference of wavefunction can occur and thus no phase can be picked up in such a open path. (2) For the ΠQW system as shown in solid curves in Figs. 7(a) and (b), both cases show a one-to-one correspondence to each other. This manifests that the influence of magnetic field on the transmission profile depends only on the magnetic field strength. However, there is no correspondence in the case of ΠCQW which is presented by the dotted lines in Figs. 7(a) and (b). (3) Generally speaking, opposite polarity of the magnetic field causes different influence on the transmission in ΠCQW systems.

The transmission profiles versus Fermi wave number k_F for the case that the magnetic field being applied to both regions II and V, are displayed in Fig. 8. Fig. 8(a) presents the transmission in the ΠQWs and ΠCQWs with same polarity in both vertical arms, and Fig. 8(b) presents those with opposite polarity to each other in two vertical arms. The curves are offset for clarity. The solid lines represent the ΠQW system and dotted lines represent the ΠCQW system. It is found that for ΠQW case, though the geometry and the applied field are symmetric, the transmission probabilities are different from each other (e.g. the solid curves with $v = 0.2$ and -0.2) as can be seen from Fig. 8(a). However, for ΠCQW case, the transmission is polarity independent as can be noted from the dotted curves in Fig. 8(a). No such symmetry can be found in ΠCQW as shown in Fig. 8(b). Furthermore, peak-dip structures are evident both in Figs. 8(a) and (b) at high field situations, though the electrons always move in field free region. One can expect that the transmission profiles will become stepwise structures when the applied magnetic field is extremely high. And in the intermediate field strength, the magnetic field changes the oscillatory behavior of the profiles significantly.
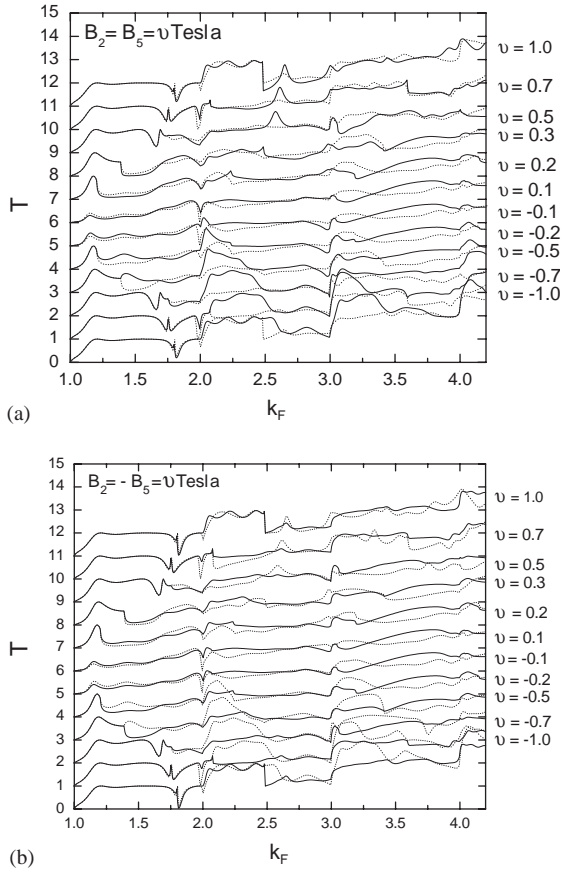
Fig. 8. Transmission profiles versus k_F for the magnetic field applied to both vertical arms. (a) same polarity, and (b) opposite polarity in II and V. The solid lines represent the T of ΠQW, while the dotted lines represent the T of ΠCQW. Two consecutive curves have been offset vertically for clarity.

oscillatory behavior as the distance d is increased and manifest periodic features as the distance d is varied. T-shaped quantum wires have been proposed to achieve the quantum interference effect by controlling the length of its lateral closed arms. In the present study, it is found that the interference pattern can be easier to obtain by modulating the length and width of transversal arms and the distance between two arms.

When a potential is added to the connection region, it results in decoupling or coupling effects between the two TQWs according to whether it is positive or negative. This behavior is observed by the alternating occurrence of the successive dips and valleys when the potential is increased positively. When magnetic field is applied on the vertical arms, though the electrons pass through only the field free region, the magnetic field still affects the transmission in the QWs profoundly. The perfect transmission can be seen only in the high magnetic field region.

Acknowledgements

4. Summary

In the present work, the transmission properties of the coupled TOQWs are found to be very sensitive to the geometric configurations as well as the strength and polarity of the applied fields. A double resonance is observed on the profiles at certain ratio of the width of vertical wire to horizontal wire. The transmission is suppressed drastically as the width of one or both vertical wires become large. Most of the transmission profiles of ΠQW and ΠCQW are distinguishable even for large inter-distance d between the two vertical wires. The transmission profiles exhibit

References

[1] W. Wegscheider, L.N. Pfeiffer, M.M. Dignam, A. Pinczuk, K.W. West, S.L. McCall, R. Hull, Phys. Rev. Lett. 71 (1993) 4071.

[2] Y. Hayamizu, M. Yoshita, S. Watanabe, H. Akiyama, L.N. Pfeiffer, K.W. West, Appl. Phys. Lett. 81 (2002) 4937.

[3] T. Someya, H. Akiyama, H. Sakaki, Phys. Rev. Lett. 76 (1996) 2965.

[4] D. Brinkmann, G. Fishman, Phys. Rev. B 56 (1997) 15211.

[5] A.N. Forshaw, D.M. Whittaker, Phys. Rev. B 54 (1996) 8794.

[6] M.H. Szymanska, P.B. Littlewood, R.J. Needs, Phys. Rev. B 63 (2001) 20 5317.

[7] Y.K. Lin, Y.N. Chen, D.S. Chuu, Phys. Rev. B 64 (2001) 193316;
Y.K. Lin, Y.N. Chen, D.S. Chuu, J. Appl. Phys. 91 (2002) 3054.

[8] F. Sols, M. Macucci, U. Ravaili, K. Hess, J. Appl. Phys. 66 (1989) 3892;
F. Sols, M. Macucci, Phys. Rev. B 41 (1990) 11887.

[9] J. Wang, H. Guo, Appl. Phys. Lett. 60 (1992) 654.

[10] R. Sordan, K. Nikolic, Appl. Phys. Lett. 68 (1996) 3599.

[11] G. Goldoni, F. Rossi, E. Molinari, Appl. Phys. Lett. 71 (1997) 1519.

[12] J.L. Bohn, Phys. Rev. B 56 (1997) 4132.

[13] K. Nikolic, R. Sordan, Phys. Rev. B 58 (1998) 9631.

[14] B.-Y. Gu, Y.K. Lin, D.S. Chuu, J. Appl. Phys. 86 (1999) 1013;
K.-Q. Chen, B.-Y. Gu, Y.K. Lin, D.S. Chuu, Intl. J. Mod. Phys. B 13 (1999) 903.

[15] J. Goldstone, R.L. Jaffe, Phys. Rev. B 45 (1992) 14100.